


# Modelling the competition between photo-darkening and photo-bleaching effects in high-power ytterbium-doped fibre amplifiers

A. Jolly<sup>1,2</sup>  · C. Vinçont<sup>1</sup> · Ch. Pierre<sup>1</sup> · J. Boulet<sup>1</sup>

Received: 28 February 2017 / Accepted: 1 August 2017 / Published online: 10 August 2017  
© Springer-Verlag GmbH Germany 2017

**Abstract** We propose an innovative, fully space–time model to take into account the seed-dependent nature of ageing penalties in high-power ytterbium-doped fibre amplifiers. Ageing is shown to be based on the on-going competition between photo-darkening and photo-bleaching phenomena. Our approach is based on the natural interplay between the excited states of co-existing ytterbium pairs and colour centres in highly doped fibres, in the presence of thermal coupling between the closely spaced excited states. As initiated from *IR* photons, the excitation of colour centres up to the UV band is supposed to be governed by multi-photon absorption. The interactions of interest in the kinetics of photo-bleaching then take the form of highly efficient charge transfers, which imply the reduction of some fraction of the basically trivalent ions to their divalent state. Due to the activation of ytterbium pairs by means of energy transfer up-conversion, these interactions get more and more effective at elevated operating powers. Computational results using these principles actually help to fit our experimental data regarding seeding effects, as well as fully generic trends already evidenced in the literature. This gives a fine demonstration for the need to discriminate co-active pump and signal contributions. Our self-consistent, still simplified model then consists of a valuable tool to help for a deeper understanding of the ageing issues. Furthermore,

considering higher-order ytterbium aggregates, this should open new routes towards more comprehensive models.

## 1 Introduction

Photo-darkening phenomena in fibres always imply critical penalties [1, 2] in terms of the optical performance and of the robustness of ytterbium-doped fibre amplifiers (YDFA). These are major issues in the regime of high operating powers. In the most recent large-mode area (LMA) fibres, earlier ageing effects usually appear in the range of 100–150 W after some tens of hours of operation. Despite the huge amount of research in the field during the last decades, the actual physics involved in the ageing processes and the identification of relevant parameters still leads to open discussions in numerous cases. A number of contributing mechanisms are referred to in the global forms of photo-darkening (PD) and of photo-bleaching (PB). These phenomena are governed by the kinetics of the colour centres (CC) induced in the ytterbium-doped fibre (Yb fibre). The CCs are originated from infrared pump and signal photons, in the regime of elevated laser intensities. Most often, the mechanisms of PD and PB have been considered apart. A few recent works nevertheless proved possible interactions [3, 4], either in the case of additional seeding in the visible band or of thermal post-treatment. Furthermore, surprisingly, we did not find any comprehensive, fully space–time model in the literature to help for a global analysis of the CC-dependent effects and for the management of ageing penalties. This applies, more especially, to fitting representative experimental data and to the discussion of actual optical penalties prior further optimization. In this study, we demonstrate a new model which provides a self-consistent description of the ageing process given specified pump and seed conditions. Referring to

✉ A. Jolly  
alain.jolly@alphanov.com

<sup>1</sup> ALPhANOV, Institut d’Optique d’Aquitaine, Rue François Mitterrand, 33400 Talence Cedex, France

<sup>2</sup> CEA, Centre d’Etudes Scientifiques et Techniques d’Aquitaine, Chemin des sablières, BP2, 33114 Le Barp, France

former relevant studies [5–8] and to some of the most typical questions which still remain open nowadays, this consists of an innovative approach within the frame of space–time, saturated amplification.

Our paper is organised in five gradual steps. First, we present a series of experimental results of interest for preliminary benchmark. The needs to discriminate pump and signal contributions and to pay attention to fast kinetics are evidenced. In a second step, basic physics is referred to in view of appropriate modelling assumptions. Third, for consistency with our experimental data and well-established trends in the field, the ageing kinetics is considered, thanks to a couple of competing terms. They refer to co-operating PB and PD, within the frame of a fully generic space–time approach. This leads to the defining acceptable ranges of values for the specification of the parameters involved, in the form of dedicated rates for energy transfer and charge transfer, as well as of cross sections for colouring and for subsequent optical absorption by the CCs. In a fourth step, we present parameterized series of computational plots to make sure of very generic trends due to the ageing phenomena in an YDFA and of the additional, CC-dependent thermal gradients. This also helps to comment former works of interest. In a final step, thanks to integrating the space–time computational data provided, we establish appropriate fits with benchmarked measurements. This helps to validate the principle of our model, even though simplified, and to verify the orders of magnitude suggested.

## 2 Experimental data regarding seed-dependent ageing phenomena

Let us then start with the ageing sequence of reference for experimental benchmarking. This applies to the analysis of seed effects. We aim to demonstrate the fundamental need for discriminating pump and signal contributions, in terms of ageing. The measurements are performed by combining two kinds of complementary sources for seeding the YDFA, under the condition of a constant average power, whatever the configuration. The first source is pulsed, while the second one is continuous wave (CW). The pulsed seed source delivers 60-ps-long pulses at the pulse repetition frequency (PRF) of 40 MHz. Our experimental setup makes use of a standard, highly doped LMA fibre from NKT Photonics\* (ref. NKT 40-200) in a co-propagative design [9]. The pump and output signal powers lie in the ranges of 160 and 110–120 W, with respective wavelengths close to 976 and 1064 nm. A particular attention was paid for operating the YDFA slightly below the so-called threshold of modal instability [2].

Early ageing is operated in the regime of pulsed seeding, as shown in Fig. 1. The variations of the output power and of

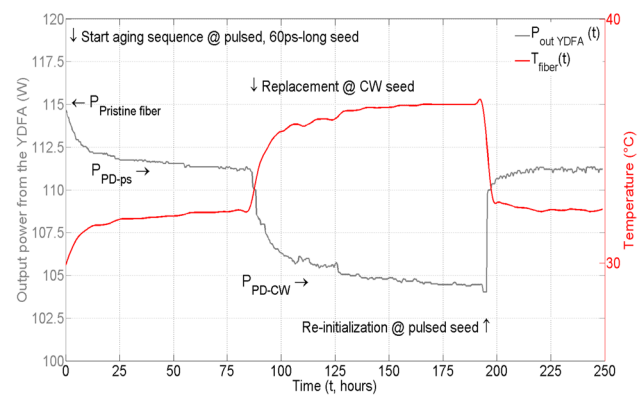


**Fig. 1** Ageing sequence, starting with 60-ps-long seed pulses, then replacing with CW seeding and re-initializing, to monitor the optical power (grey) and the temperature of the fibre (red)

the peak temperature along the fibre are monitored continuously, at the same time, during several hundred hours. Stabilised ageing being established after nearly 100 h, the pulsed seed is then replaced with its CW counterpart to verify the subsequent ageing features. The chronograms in Fig. 1 reveal the dependency of the ageing rate with the seed regime, together with the correlation between power and thermal gradients. By comparison with pulsed seeding, CW seeding leads to a significant enhancement of the ageing rate and of the temperature of the fibre. The supplementary amounts of excess loss at 1064 nm and subsequent, additional fibre-heating are in the order of ~6–7 W and 5–6 °C, respectively. It must be underlined, to the best of our knowledge, that the need to separate pump and signal-induced contributions for modelling had never been proved in such a way.

Then, it is worth to discuss the nature of the physical mechanisms involved in the generation of CCs and for annealing, which appears as a fundamental question for explaining somewhat surprising features at first thinking.

## 3 Proposal for a self-consistent model

Reminding usual basics, the early mechanism to be invoked is pure ground state absorption (GSA) from the fundamental level, for both pump and signal photons, given a three-level-based system. Further mechanisms of interest [10–14] consist of multi-photon absorption (MPA), of energy transfer up-conversion (ETU) and electronic charge transfer (CT). The MPA is consistent with energy conversion [15] from the IR to the UV band. Indeed, still being originated by pump and signal photons, the ageing process produces CCs with characteristic energies up to several eVs. This is a non-resonant process, as well as CT which goes with pure ionisation [16], either in the form of electron capture or of electron release. On the contrary, ETU is a resonant

process. Regarding Yb pairs, this implies a gap of which the value is twice the photon or signal energy, depending upon the source term. The physical origin of CCs actually depends upon the nature of intrinsic defect centres in the host silica and of extrinsic species contained, including possible co-doping. The intrinsic centres are determined by specific internal bonds. The most classical examples [17] to be reminded are oxygen-deficient centres (ODCs), peroxy-radical centres (POR) or other hole centres (NBOHCs), or oxygen hole centres (OHCs). In our experimental setup, we will focus on aluminium ions (Al-OHCs) [18, 19], as part of the specified co-doping. The behaviour of this kind of defects is governed by the physics of ligand-based and oxygen-related para-magnetic species, interstitials and vacancies in the matrix of reference.

Because the detailed analysis of the actual nature of centres involved remains out of the scope of our paper, we just make use of the very generic, former mechanisms in connection with macroscopic data for parameterization. This impacts on to the use of MPA by means of an equivalent value of the global absorption cross section, and on ETU when determining the rate of energy transfer from the range of excited levels associated with the pump and with the signal towards the virtual states of Yb pairs. A number of published studies have been devoted to the issue of Yb<sup>3+</sup> aggregation [7, 20] in the presence of elevated concentrations for fibre-doping ( $N_{tot}$ ). In their simplest form, the aggregates consist of trivalent pairs. Even though higher-order Yb species should be actually considered [7] in view of more comprehensive modelling, we assume that the

pairs remain the most probable and most efficient contributors. To set up the basis of our model, we consider a global interplay between single Yb<sup>3+</sup> ions, single Yb<sup>3+</sup> pairs and MPA-originated CCs. This is assumed within the frame of highly efficient CT, which arises from thermally induced, natural energy transfers between closely spaced ions and neighbouring excited states across the gap. The actual rate of CT determines the actual equilibrium between PD and PB; the former being originated from MPA and the latter from CT in the presence of pump-induced ETU towards Yb<sup>3+</sup> pairs. While lasing, this characterises some kind of on-going competition [10]. Unlike previous works where very different interactions have been proposed between other co-existing species, a specific attention is paid to the critical concern of a fast kinetics in the energy diagram (Fig. 2).

The transitions undergone by useful, single Yb<sup>3+</sup> ions and Yb<sup>3+</sup> pairs are figured in the first two sub-diagrams on the left-hand side. The other two sub-diagrams on the right-hand side apply to the CT-dependent transitions of interest for CCs and to the generation of Yb<sup>2+</sup> species [20]. In the same way as MPA, as already mentioned, ETU is assumed to originate from both pump and signal photons (Fig. 2, left-hand side). According to this energy diagram and the associated physics, we can develop a fully space-time computational model to describe the ageing penalties under representative conditions. This is done versus the geometrical data and the operating conditions of the YDFA, in a close connection with the requirements for a fast kinetics. A global set of equations to describe the

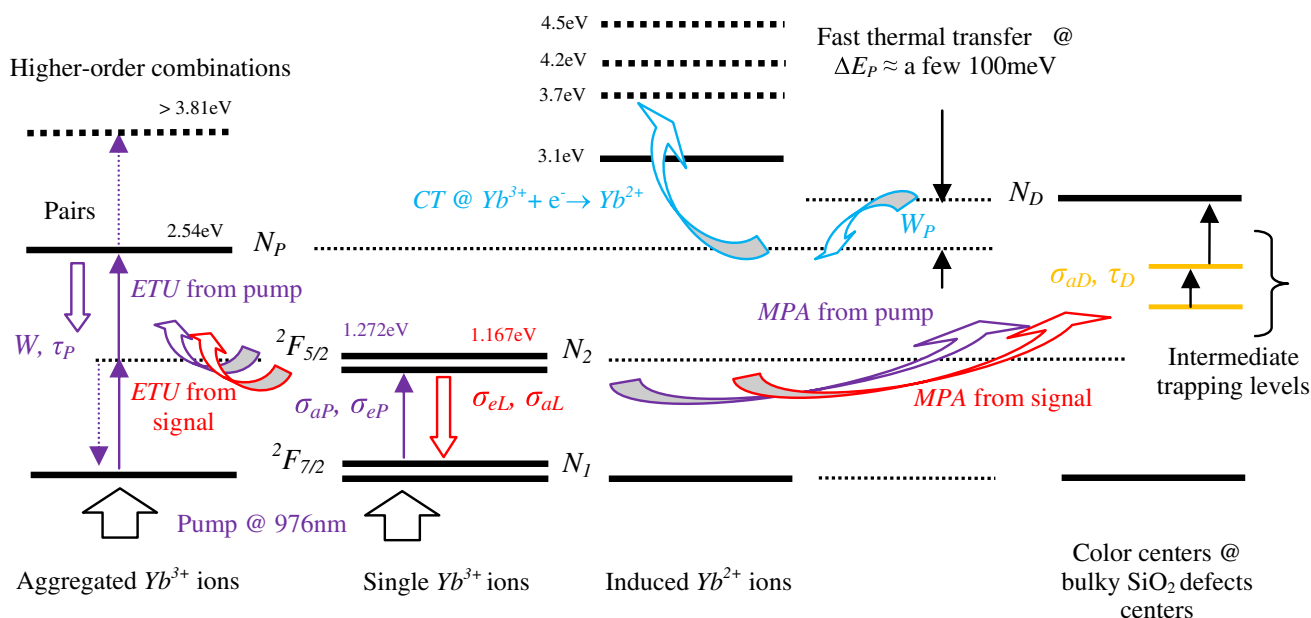


**Fig. 2** Interplay between the excited states of Yb<sup>3+</sup> pairs and colour centres, as originated from co-operating pump (purple) and signal (red) powers

propagation of pump and signal powers along the fibre, while accounting for the combined effects of ETU, MPA and CT is as follows:

$$\frac{\partial P_P}{\partial z} = -\Gamma_P \{ \sigma_{ap} [N_{tot} - N_2] + \sigma_{aCC} N_D + \alpha_p \} P_P \tag{1}$$

$$\frac{\partial P_S}{\partial z} = +\Gamma_S \{ \sigma_{eL} N_2 - \sigma_{aL} [N_{tot} - N_2] - \sigma_{aCC} N_D - \alpha_S \} P_S \tag{2}$$

$$\begin{aligned} \frac{\partial N_2}{\partial t} = & + \frac{\Gamma_P \sigma_{ap} P_P + \Gamma_S \sigma_{aL} P_S}{h\nu A} [N_{tot} - N_2] - \frac{\Gamma_S \sigma_{eL} P_S}{h\nu A} N_2 \\ & - \frac{N_2}{\tau_F} - 2WN_2^2 - \frac{\sigma_{aD} (\Gamma_P P_P + \Gamma_S P_S) N_2}{h\nu A} \end{aligned} \tag{3}$$

$$\frac{\partial N_P}{\partial t} = WN_2^2 + \frac{W_P}{2} N_P N_D - \frac{N_P}{\tau_P} \tag{4}$$

$$\frac{\partial N_D}{\partial t} = \frac{(\Gamma_P P_P + \Gamma_S P_S) \sigma_{aD}}{h\nu A} N_2 - W_P N_P N_D - \frac{N_D}{\tau_D} \tag{5}$$

Equations (1, 2) describe the spatial balance of pump and signal ( $P_P, P_S$ ) power gradients along a fibre where the length and the core area are denoted  $L$  and  $A$ , respectively. Equations (3–5) figure the rate terms. The densities of excited  $\text{Yb}^{3+}$  ions,  $\text{Yb}^{3+}$  pairs and  $\text{Yb}^{2+}$  species are denoted  $N_2, N_P$  and  $N_D$ , respectively.  $W$  ( $\text{m}^3/\text{s}$ ) describes the rate of ETU towards the  $\text{Yb}^{3+}$  pairs. Orders of magnitude of further interest for  $W$  may be referred to those of other media, for example a few parts to some  $10^{-17} \text{ cm}^{-3}/\text{s}$  as in the case of Er–Yb co-doped silica. The notations  $\sigma_{aCC}$  and  $\sigma_{aD}$  apply to the cross sections for optical absorption by CCs and global MPA, while  $W_P$  ( $\text{m}^3/\text{s}$ ) figures the rate of CT from the CCs to excited  $\text{Yb}^{3+}$  pairs. The closest the excited states of  $\text{Yb}^{3+}$  pairs and CCs, the more efficient the process of CT. The lifetimes for characterizing the isolated and paired  $\text{Yb}^{3+}$ -species, as well as divalent ions [21, 22], are  $\tau_F \approx 1 \text{ ms}$ ,  $\tau_P \approx \tau_F/2$  and  $\tau_D \approx 100 \mu\text{s}$  [22], respectively. The set of more standard cross sections for quantifying the lasing performance, i.e.  $\sigma_{ap}, \sigma_{aL}, \sigma_{ep}$  and  $\sigma_{eL}$ , is governed by usual numbers from the spectroscopy of single  $\text{Yb}^{3+}$  ions in pure silica. They characterise the optical absorption and emission, or re-emission at the pump and laser wavelengths. The coefficients  $\alpha_p$  and  $\alpha_S$  denote passive losses ( $\text{m}^{-1}$ ) prior ageing, out of any excess loss due to additional PD. Let us start by setting  $\frac{\partial}{\partial t} = 0$  in (7–9). This gives the suitable expressions for  $N_2, N_P$  and  $N_D$  in the CW mode of operation, before solving (1, 2). To identify analytical solutions, we start by defining two quantities  $N$  and  $S$  in respective units of  $\text{m}^{-6}$  and  $\text{m}^{-3}$ , as follows:

$$S = \frac{1}{W} \left[ \left( \frac{\rho_T}{h\nu A} + \frac{1}{\tau_F} \right) \left( 1 + \frac{\tau_P}{2\tau_D} \right) - \frac{\rho_{MSA}}{2h\nu A} \right], \tag{7}$$

where the three factors in the former expressions are pump- and signal-dependent, i.e.  $\rho_T = (\Gamma_P P_P + \Gamma_S P_S) \sigma_{aD} + \Gamma_S P_S (\sigma_{eL} + \sigma_{aL}) + \Gamma_P P_P \sigma_{ap}$ ,  $\rho_{MSA} = (\Gamma_P P_P + \Gamma_S P_S) \sigma_{aD}$  and  $\rho_A = \Gamma_P P_P \sigma_{ap} + \Gamma_S P_S \sigma_{aL}$ .

They are specified in  $\text{W m}^2$ . According to these notations, the three CW solutions of interest can be written in the following form:

$$N_2 = \frac{(N - S)}{2 \left( 1 + \frac{\tau_P}{2\tau_D} \right)} \tag{8}$$

$$N_P = \frac{\tau_P}{\left( 1 + \frac{\tau_P}{2\tau_D} \right)} \left\{ \frac{\rho_A N_{tot}}{h\nu A} - \frac{(N - S)}{2 \left( 1 + \frac{\tau_P}{2\tau_D} \right)} \left[ \frac{\rho_T - \rho_{MSA}}{h\nu A} + \frac{1}{\tau_F} \right] \right\} \tag{9}$$

$$N_D = \frac{\frac{(N-S)}{2 \left( 1 + \frac{\tau_P}{2\tau_D} \right)} \left[ \frac{1}{\tau_P} + \frac{1}{W_P \tau_D} \left( \frac{\rho_T}{h\nu A} + \frac{1}{\tau_F} \right) \right] - \frac{\rho_A N_{tot}}{h\nu A W_P \tau_D}}{\frac{\rho_A N_{tot}}{h\nu A} - \frac{(N-S)}{2 \left( 1 + \frac{\tau_P}{2\tau_D} \right)} \left[ \frac{\rho_T - \rho_{MSA}}{h\nu A} + \frac{1}{\tau_F} \right]} \tag{10}$$

The gap-dependent efficiency of CT which governs the actual value of  $W_P$  may be estimated, at least qualitatively, thanks to plus or minus complex principles as predicted by Marcus theory and other deviations [24, 25] in the presence of phonon-assisted mechanisms. This involves exponentially decreasing laws as specified in the distribution of Boltzmann, to be applied to the population of thermal electrons. On another step, we also need to consider the thermal gradients along the fibre. They carry relevant information of interest for discriminating the heat sources associated with the quantum defect and to the optical absorption in excess, due to the CCs. Solving the heat equation for pure radial conduction, within specified conditions of thermal exchange from the outer clad ( $h_{ech}, \text{W}/\text{m}^2/\text{K}$ ) towards the surrounding environment ( $T_c, \text{K}$ ), we get a fairly simple expression:

$$T_{clad} = T_c + \frac{[Q_{QD} + Q_{CCP} + Q_{absP} + Q_{CCL} + Q_{absL}] R_{core}^2}{2h_{ech} R_{clad}}, \tag{11}$$

where  $R_{core}$  and  $R_{clad}$  are the core and clad radii. The notations  $Q_{QD}, Q_{CCP}, Q_{CCL}, Q_{absP}$  and  $Q_{absL}$  define the various

$$N = \sqrt{\left( \frac{\rho_{MSA}}{2W h\nu A} \right)^2 + \frac{1}{W} \left( 1 + \frac{\tau_P}{2\tau_D} \right) \left\{ \frac{1}{W} \left( 1 + \frac{\tau_P}{2\tau_D} \right) \left[ \left( \frac{\rho_T}{h\nu A} + \frac{1}{\tau_F} \right)^2 + \frac{8W \rho_A N_{tot}}{h\nu A} \right] - \frac{1}{h\nu A} \left[ \left( \frac{\rho_T}{h\nu A} + \frac{1}{\tau_F} \right) \frac{\rho_{MSA}}{W} + 4\rho_A N_{tot} \right] \right\}}, \tag{6}$$

heat sources comprised in the total heat load. They figure the quantum defect, the excess absorption due to CCs and passive absorption at the pump and laser wavelengths, respectively. All of them are computed by means of the actual value of local power gradients. The parameter  $h_{ech}$  is adjusted in such a way that Eq. (11) enables an appropriate fit of our model with the experimental results, which remains consistent as long as the selected value is kept somewhere between 10 and 100 W/m<sup>2</sup>/K.

#### 4 From the pristine fibre to the parameterization of the model

Let us go on with computational process which was developed for providing the numerical solutions of Eqs. (1–5, 11), i.e. the spatial distributions of the Yb species and of the optical powers along the fibre. The complete set of sizing data for global parameterization is composed of  $W$ ,  $W_p$ ,  $\sigma_{ad}$ , and  $\sigma_{acc}$ . Further modelling results will be based on appropriate sets comprising these four parameters, for discussing various combinations with plus or minus efficient MPA, ETU, CT and optical absorption by the CCs to be defined in the band of IR wavelengths. For discriminating the intrinsic influence of ETU given the selected doping concentration in the pristine fibre, prior significant ageing, we start by varying  $W$ . This takes place among deleterious effects to be expected in the presence of excess doping [12]. The larger fractional part of Yb<sup>3+</sup> ions comprised in the excited pairs, the stronger the reduction of the optical efficiency of the YDFA. We need to fit the actual transfer characteristic of our setup, in pristine state before ageing. Thanks to preliminary benchmark, we determined  $N_{tot} \cong 3 \times 10^{25} \text{ m}^{-3}$ . Characterising our setup, we evidenced a signal power of about 110 W for a pump power of 160 W. When varying  $W$  in the range  $10^{-20}$ – $2 \times 10^{-19} \text{ m}^3/\text{s}$ , our model then gives very consistent results (Fig. 3). This concerns the pump and signal power distribution along the fibre, as well as the subsequent trends and affordable limitations for  $N_{tot}$ . The most relevant value of  $W$  for fitting is equal to  $10^{-19} \text{ m}^3/\text{s}$ , to be considered below.

The straightforward determination of a precise set of values for  $\{\sigma_{ad}, \sigma_{acc}\}$  is not as easy as for  $W$ . Even in the case of very representative works [6–8] with closed concerns, to the best of our knowledge, this topic does not still lead to any dedicated study for reference. Furthermore, no open data could be founded using the standard datasheet of our fibre. This is the reason why we need to proceed with orders of magnitude, nevertheless quite representative estimates. In this regard, we account for the average excess loss (EL) of about 10% after stabilised ageing while considering that Eqs. (3–5) do not refer to any

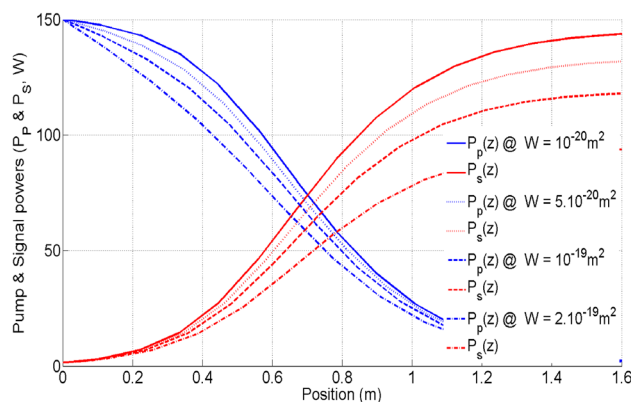


**Fig. 3** Variations of the pump and signal power distributions along the pristine fibre with the rate of excitation of Yb<sup>3+</sup> pairs by ETU

particular location along the fiber. For a rough approximation, we just make the approximation that half the pump power has been transferred to the signal power in the central area of the fibre, at  $z = L/2$ , i.e.  $P_p(L_{fibre}/2) \approx P_s(L_{fibre}/2) \approx P_{pump}/2$ . This figures the case of an optimised design for the YDFA with nearly zero emerging pump and complete power transfer at the output of the fibre.

Referring to (8–10), to a set of consistent values for  $\sigma_{acc}$  and ranging  $\sigma_{ad}$  over several decades (Fig. 4), the variations of  $EL(\sigma_{ad}, \sigma_{acc})$  are determined within a broad range of values. This method helps to evidence generic trends and orders of magnitude in the presence of arbitrary large variations of the  $EL$  during  $PD$ , versus applicable sets of values  $\{\sigma_{ad}, \sigma_{acc}\}$ . In the following, we will use  $\{\sigma_{ad}, \sigma_{acc}\} = \{10^{-27} \text{ m}^2, 10^{-23} \text{ m}^2\}$  as the central values of interest for appropriate fits.

The data describing pure kinetics are contained in the sub-system of Eqs. (3–5), which can be easily solved versus the pulse shape of the seed. At this step, we aim to focus on the role of the rate of CT and explain the duty-cycle (DC) effects in Fig. 1.

Paying attention to the definition of the suitable initial conditions for figuring the regime of equilibrium, in accordance with (6–10), we get the results in Fig. 5. This already shows that a few ns-long transition times are made possible given acceptable values for  $W_p$  from  $10^{-19}$  to  $10^{-18} \text{ m}^3/\text{s}$ . For more precise fits, we still need to compute the time integral of the flashes of CCs', to be related to the actual PD transients of interest. This provides the value of the ratio ( $\eta$ ) of the average seed contribution to the total initial power, as specified in Fig. 1, in the form of  $\eta = (P_{PD-CW} - P_{PD-ps})/P_{PD-ps}$ . Similar operations are

duplicated in the two seed regimes to determine the subsequent power drop at the output of the YDFA, due to the replacement of the pulsed seed with its CW counterpart. We verified that the most relevant value for  $W_p$ , which



**Fig. 4** Variation of the total absorption loss due to the colour centres within a large range of values of  $\sigma_{aD}$ , given a rough estimate for the sensitivity to the MPA-dependent contribution

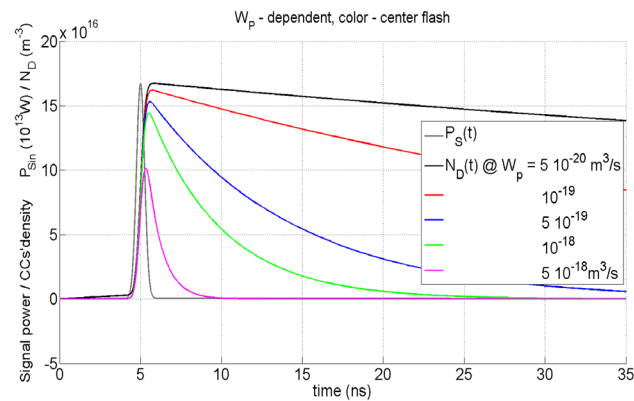
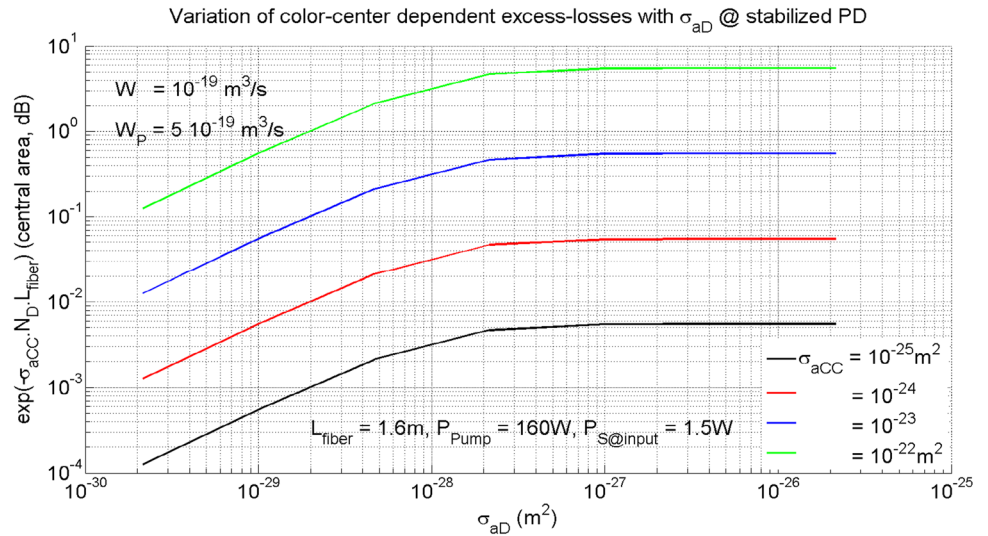


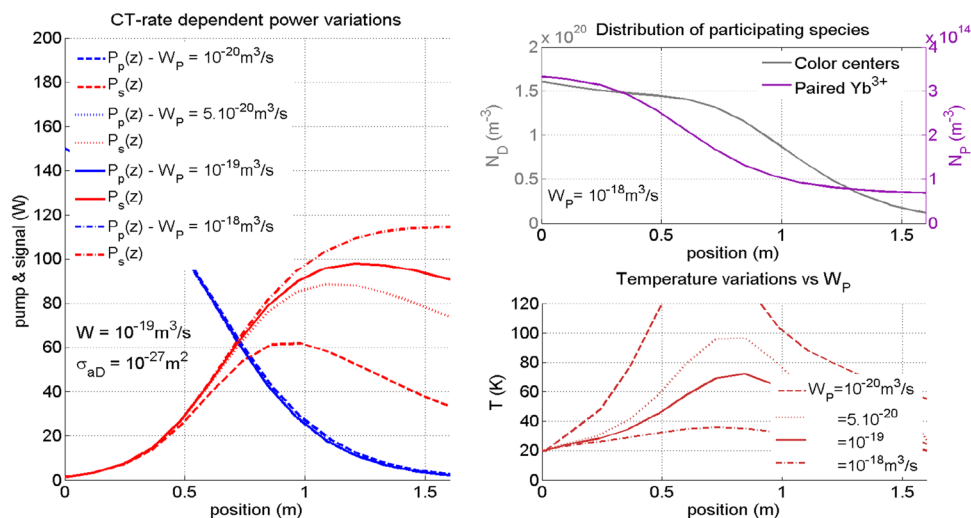
**Fig. 5** Computed PD transients due to the CCs in the presence of 60-ps-long seed pulses as a function of the ionisation rate  $W_p$

enables  $\eta \approx 5\text{--}10\%$ , lies in the range of  $2 \times 10^{-19}\text{--}7 \times 10^{-19} \text{ m}^3/\text{s}$ . These simplified calculations only apply, however, to short-term PD variations. They do not apply to long-term transients during the ageing sequence. This is consistent for properly stabilised power drops, as illustrated in Fig. 1 thanks to  $P_{PD-ps}$  and  $P_{PD-CW}$ , several tens of hours after the activation of a given seed and by reference to the pristine state. The actual kinetics of more gradual, ageing phenomena in the long term should be stated within the frame of much more complex physical mechanisms of different natures. This must be kept in mind even though, from the macroscopic point of view, higher values of  $\sigma_{aD}$  obviously ensure larger PD rates. Because of the lack of well-established physical models in the transient regime, the fitting processes rather involve arbitrary exponential-based laws, using the so-called stretching parameters with a couple of constants, or possibly more.

### 5 Space–time analysis of the ageing penalties in the YDFA and related transfer characteristics

Referring to former estimates for the orders of magnitude of the rates of ETU and CT, we look at the sensitivity of the ageing penalties to MPA and optical absorption in the CCs. This involves the output power and the optical efficiency of the YDFA, to be denoted accordingly to  $P_{Sout} = P_S(L_{\text{fibre}})$  and  $\eta_{O/O} = P_{Sout}/P_{\text{pump}}$ . Prior further integration for the analysis of input–output transfer data, we start by determining the raw distributions of  $P_S(z)$ ,  $P_P(z)$ , and of the other species along the fibre. Our computations will be parameterized versus  $W_p$  and  $\sigma_{aD}$ , to show the consistency of the model with expected trends. Let us consider high-quality silica in the situation where variations of the excess loss are essentially governed by those of the optical absorption in excess due to CCs. Given excess losses of about 1–2 dB to remain in agreement with our experimental data, the computational results provided in Fig. 4 are consistent with the former orders of magnitude, i.e.  $\sigma_{aD} \approx 10^{-27} \text{ m}^2$  and  $\sigma_{aCC} \approx 10^{-23} \text{ m}^2$ . Starting from the computed distributions of the optical powers, other species and thermal gradients along the fibre (Fig. 6), we determine the sensitivity of the YDFA to variations of the rate of CT and subsequent penalties in terms of optical efficiency. Let us denote the former quantities as  $P_S(L_{\text{fibre}})$  and  $\eta_{O/O} = P_S(L_{\text{fibre}})/P_{\text{pump}}$ , respectively. As long as  $W_p$  remains in excess of a few  $10^{-19} \text{ m}^3/\text{s}$  (Fig. 6, left-hand side),  $\eta_{O/O}$  decreases no more than 15%. But unaffordable penalties tend to appear, as soon as  $W_p$  tends to decrease below  $10^{-19} \text{ m}^3/\text{s}$ . As expected, we verify a great sensitivity to CT. Here again, this illustrates the principle of on-going competition between PD and PB regarding the regime of equilibrium. An accurate prediction of the optical performance of the YDFA, while ageing, must then be based on the knowledge of the appropriate value for  $W_p$ .

**Fig. 6** Variations of the spatial distribution of the pump and signal powers (*left*), of the density of ionic species (*top-right*) and of the peak temperature in the fibre with the rate of CT (*bottom-right*)



On another step, the peak densities of CCs are founded in the area of the fibre input closed to the pump, as expected in a co-propagative pump architecture (Fig. 6, top right-hand side). This is the location of more deleterious PD. The profiles of  $N_p(z)$  and  $N_D(z)$  then match those of  $P_p(z)$ . In the favourable situation of  $W_p = 10^{-18} \text{ m}^3/\text{s}$ , they undergo plus or minus rapid decreases towards the output, by a factor of more than 10 for  $N_D$ , and of about 5 for  $N_p$ . Another interesting feature must be underlined at this step, when considering the product  $\sigma_{aCC} \times \langle N_D \rangle$ . Given the value of the absorption cross section, deduced thanks to fits using experimental data from [18], and  $\langle N_D \rangle$  the averaged value of computed PD transients, we also confirm representative numbers with the literature. The orders of magnitude computed for  $\langle N_D \rangle$ , in the range of  $10^{19}$ – $10^{20} \text{ m}^{-3}$ , correspond to the expected values for  $\sigma_{aCC} \times \langle N_D \rangle$ , i.e. about  $10 \text{ m}^{-1}$ . These estimates are specified for IR wavelengths, referring to the spectral distribution of  $\text{Yb}^{2+}$ -dependent absorption spectra. The peak thermal gradients and peak pump gradients are located in the same area of the fibre, not too far from the middle for an optimised design (Fig. 6, bottom right). Their location may vary somewhat with lasing conditions and sizing, versus the selected length of fibre, and versus the doping content or pump power specified. As shown, the convenient value for fitting our experimental results in the range of 30–40 °C is  $h_{ech} = 60 \text{ W/m}^2/\text{K}$ . The computations inferred also indicate rapid variations of the peak temperature with the rate of CT. As soon as  $W_p$  is kept higher than a few  $10^{-19} \text{ m}^3/\text{s}$ , the additional gradients do not exceed 30 °C. But the reduction of  $W_p$  below  $10^{-20}$ – $10^{-19} \text{ m}^3/\text{s}$  leads to prohibitive values of the peak temperature, in excess of 150 °C. This may imply accelerated ageing, or even catastrophic damage in the area of the fibre clad. The connection between power gradients and thermal gradients and their respective magnitudes, here evidenced, then suggests possible directions for improving the robustness of the amplifier. A properly designed,

bi-directional pumping architecture might offer a relevant alternative.

Assuming  $W_p = 10^{-19} \text{ m}^3/\text{s}$  to take advantage of efficient CT and go on with fast kinetics, now it is worth to look at the sensitivity to MPA. As long as  $\sigma_{aD}$  does not exceed  $10^{-27}$ – $10^{-26} \text{ m}^2$  (Fig. 7, left-hand side), there is no noticeable decrease of  $\eta_{o/o}$ . By reference to the pristine fibre, the attainable output power then essentially remains  $W$  dependent. This figures the case of defect-free silica. But rapidly increasing penalties gradually appear in the range of  $\sigma_{aD} = 10^{-26}$ – $10^{-25} \text{ m}^2$ . Similar trends as before are verified in the favourable case of the combination of a low density of defects and of highly efficient CT with  $W_p = 5 \times 10^{-17} \text{ m}^3/\text{s}$ . When scanning the fibre length from the input to the output of the YDFA (Fig. 7, top right-hand side), the densities of Yb pairs and CCs also undergo a strong decrease, by a factor of 6–8 and by a factor of nearly 3, respectively. The former is not as large as it was in Fig. 6, which indicates less critical thermal issues. Nevertheless, the strong dependency of the reduction of the optical efficiency with elevated values for  $\sigma_{aD}$  cannot be related to a noticeable increase of the thermal gradients (Fig. 7, bottom right-hand side).

Thanks to the integration of computational values from the input to the output of the fibre, it is possible to look at the shape of two kinds of specific characteristics of interest for the global discussion of our model (Fig. 8). The first, in the form of  $P_S(L_{\text{fibre}}, P_{\text{pump}})$ , consists of the input–output, transfer characteristic, which determines the optical efficiency for a given  $P_{\text{pump}}$  (Fig. 8, left-hand side). The second, in the form of EL ( $N_2/N_1$ ), is the excess-loss characteristic. The latter characteristic and its variations have been the topic of previous works [23], because its shape sets up a useful signature. In our model, this can be verified the same way. The larger inversion ratio, the lower amount of excess loss. Plus or minus quadratic variations (Fig. 8, right-hand side) appear within certain conditions, to be more especially related with

**Fig. 7** Variations of the spatial distribution of the pump and signal powers (*left*), of the density of Yb species (*top-right*) and of the peak temperature of the fibre (*bottom-right*) with the cross section of MPA

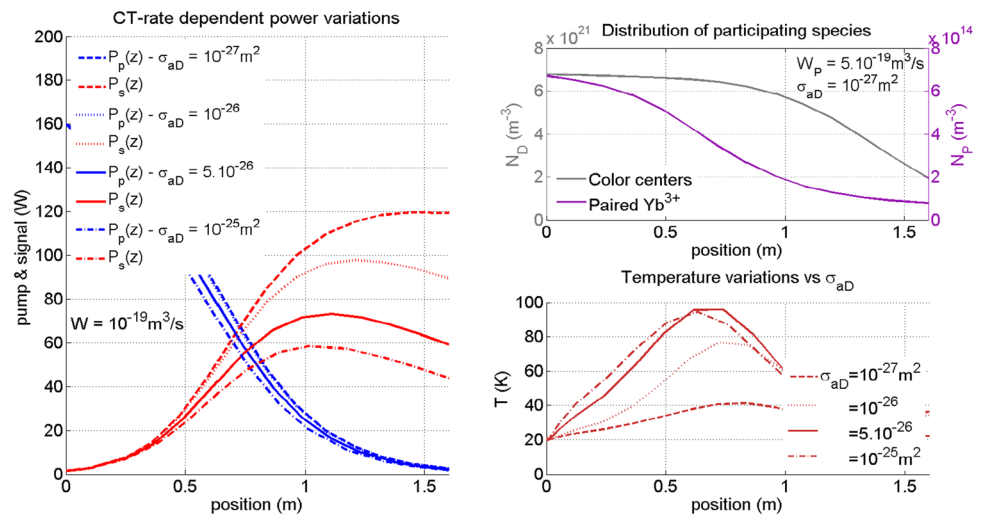
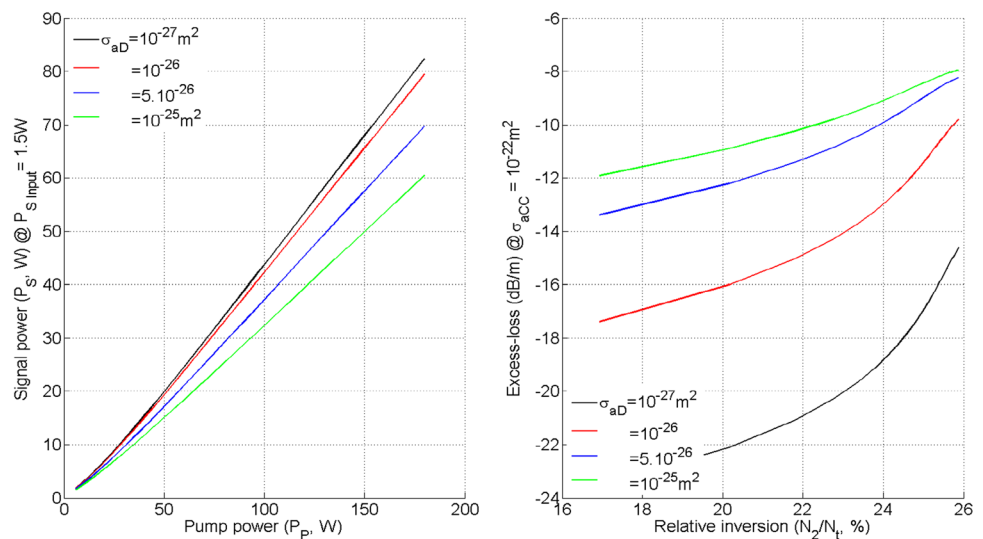


**Fig. 8** Transfer characteristic (*left*) and loss characteristic of the YDFA as a function of the inversion ratio (*right*) given the absorption cross section for MPA



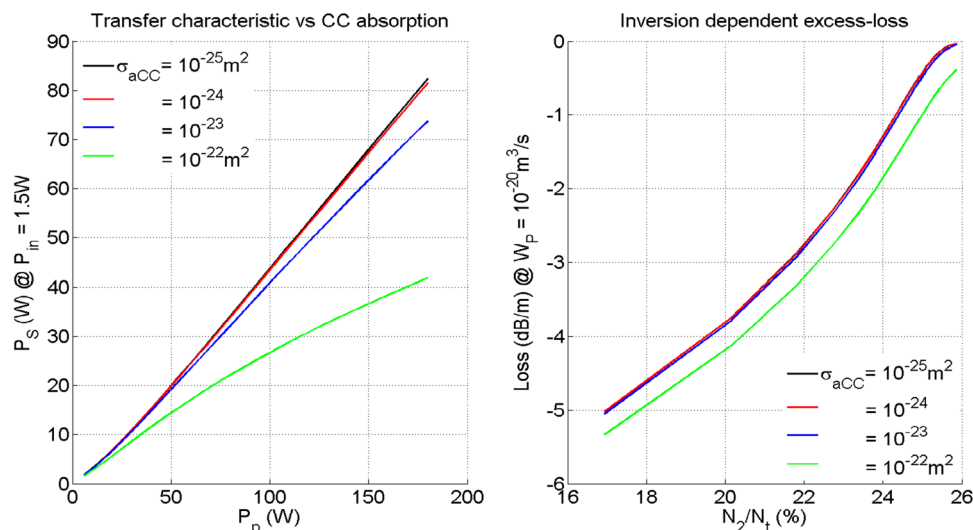
the case of a low defect content and fairly moderated optical penalties. This applies for values of  $\sigma_{aD}$  below  $10^{-26} \text{ m}^2$ , typically. The discrepancies between the actual shape of EL ( $N_2/N_t$ ) and a pure quadratic profile come from the relative contribution of CT to the global equilibrium between PD and PB along the active fibre, which varies with the operating conditions of the YDFA. The initiation of rather severe penalties when  $\sigma_{aD}$  reaches a few  $10^{-26} \text{ m}^2$  appears to be related to a reduction of the nonlinearity of the loss characteristic.

For referring to the influence of Yb pairs, the nearly quadratic variations to be noticed for lower values of  $\sigma_{aD}$  appear to be in a good agreement with [23]. In terms of global ageing variations, we must not forget that global optical penalty necessarily results from a combination of the effects of  $\sigma_{aCC}$  and  $\sigma_{aD}$ . Thus, the same way as already done for  $\sigma_{aD}$ , we need to vary  $\sigma_{aCC}$  and discriminate the two contributions. This will help to make sure of the most deleterious. Despite

the initiating process from excited states and subsequent peak value in the UV band, the value of  $\sigma_{aCC}$  needs to be referred to in the IR. This ensures a convenient definition of the excess absorption associated with CCs, in connection with homogeneous broadening features. Due to the close spacing between the pump and signal wavelengths, we just define a unique  $\sigma_{aCC}$ . Considering the IR band, already published orders of magnitude in various fibre designs indicate very variable values of  $\sigma_{aCC}$ , somewhere between  $10^{-25}$  and  $10^{-22} \text{ m}^2$ . For benchmarking, anything else being the same, the particular contribution of the CCs to PD is evidenced while varying  $\sigma_{aCC}$  over three decades (Fig. 9), throughout the range of values already considered in Fig. 4. As long as  $\sigma_{aCC}$  does not exceed a couple of  $10^{-23} \text{ m}^2$ , its fractional contribution to the global penalty remains negligible (Fig. 9, left-hand side) and the loss characteristic is kept nearly unchanged (Fig. 9, right-hand side). But very severe degradations occur towards  $\sigma_{aCC} \approx 10^{-23} - 10^{-22} \text{ m}^2$ , with a



**Fig. 9** Transfer characteristic (left) and loss characteristic of the YDFA as a function of the inversion ratio (right) given the absorption cross section of colour centres



threshold-like tendency. By comparison with those observed when ranging  $\sigma_{aD}$ , they do not appear to be associated with very significant variations of the excess-loss characteristic. When increasing  $\sigma_{aCC}$  up to  $10^{-23} \text{ m}^2$ , this characteristic is just shifted by a constant value, typically a fraction of dB/m. Despite the reduction of the optical efficiency of the YDFA by a factor of about two, its shape remains unchanged.

Beyond consistent trends, we must underline that our model also helps to verify formerly published data regarding the absorption of  $\text{Yb}^{2+}$ -related CCs associated with Al-OHC centres [19]. We verify the orders of magnitude to be expected in the IR band in the presence of this kind of species. Using  $\sigma_{aCC} \times N_D$  for an estimate of the excess absorption, it can be shown that the computed values for  $N_D$  are quite consistent with absorption coefficients between 10 and  $50 \text{ m}^{-1}$ , as indicated for a photon energy of  $\approx 1.5 \text{ eV}$ .

Finally, the apparent discrepancy to be noticed between the rapid decrease of  $\eta_{O/O}$  which results and the rather low reduction of excess loss, while increasing  $\sigma_{aCC}$  up to  $10^{-22} \text{ m}^2$ , can be explained by the integration process along the fibre. This tends to minimise the influence of roll-off near the fibre output.

## 6 Fitting seed-dependent ageing-rate variations

To set up consistent conditions for fitting the experimental data in Fig. 1 with our model in the transient regime, accordingly to Fig. 5 and the value specified for  $W_p$ , we need to make use of the seed-dependent contribution the proper way. In this respect, a DC-dependent coefficient ( $C_{DC}$ ) must be added in (1, 2), in factor of  $\sigma_{aCC}$ , prior combining the solutions of the complete system of Eqs. (1–5) with expressions (6–10) and (11). Due to the need for temporal integration in the CW regime, the updated computational process

ensures a rigorous description of the competing phenomena of PD and PB accordingly to the diagram in Fig. 2. The fractional, pump and signal-dependent contributions to PD being clearly discriminated, we get a series of computational data which help to benchmark and to validate the model (Fig. 10). This enables us to highlight the influence of the fast transients which arise from the signal-dependent terms in the equations. A series of computational values regarding the variations of the output power from the YDFA, provided the set of specified values for  $\sigma_{aCC}$  and  $W_p$ , has been superimposed with former experimental data of reference (Fig. 10, left-hand side). This reveals that the best fit conditions for  $\sigma_{aCC}$  and  $W_p$  lie in the respective ranges of  $5 \times 10^{-23}$ – $10^{-22} \text{ m}^2$  and of  $1$ – $2 \times 10^{16} \text{ m}^3/\text{s}$ .

The corresponding distributions of the thermal gradients along the fibre have also been superimposed (Fig. 10, right-hand side), when parameterized by  $C_{DC}$  within the former assumptions already made for MPA and for the optical absorption by the CCs, that is  $\sigma_{aD} = 10^{-27}$  and  $\sigma_{aCC} = 10^{-22} \text{ m}^2$ . Considering the black and light-blue plots, which help to scan the effect of  $C_{DC}$  for the benchmark of the two seed regimes, we confirm appropriate orders of magnitude thanks to defining  $\eta = (P_{PD-CW} - P_{PD-ps})/P_{PD-ps}$ . By

reference to the experimental results in Fig. 1, fairly consistent variations of the power drop and of the thermal step are evidenced from  $-5$  to  $-6 \text{ W}$  and from  $+6$  to  $+8 \text{ }^\circ\text{C}$ , respectively. For interpretation, the replacement of the short pulse, 60-ps-long seed with its CW counterpart then matches, approximately, variations of  $C_{DC}$  from  $\approx 2$  to 100%. When fitting  $\eta$  with the data in Fig. 1 under these conditions, we essentially validate the selected option of  $\sigma_{aCC} = 10^{-22} \text{ m}^2$ .

This determines the fractional contribution of the CCs to the onset of thermal gradients during the ageing process, including the contribution of the quantum defect.

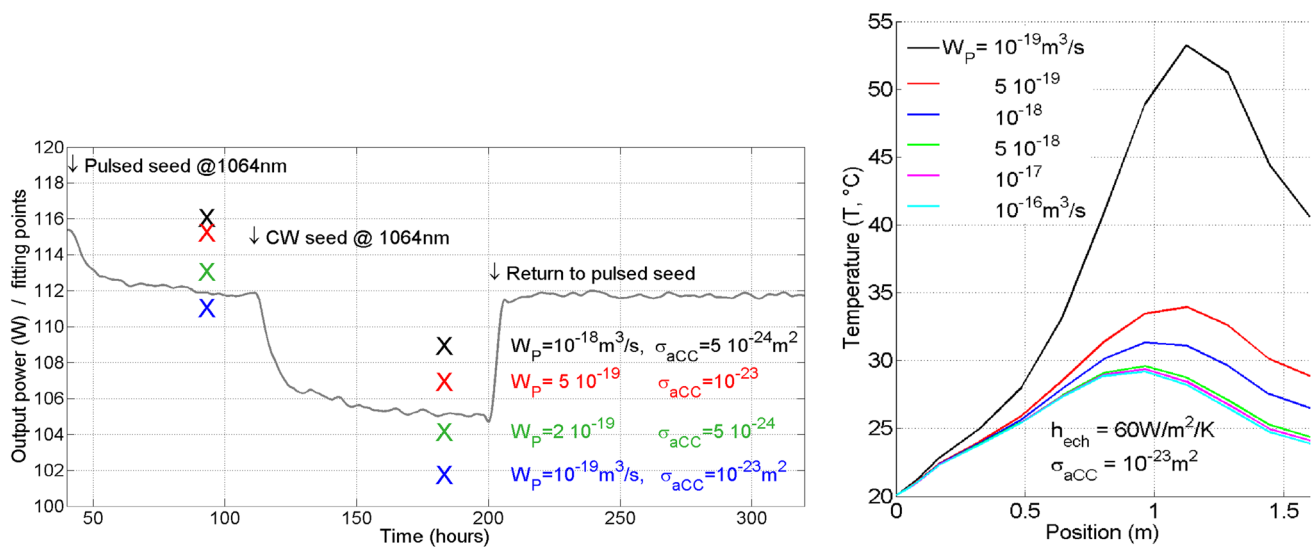


**Fig. 10** Fit of the variations of the output power from the YDFA in the CW and pulsed seed regimes with former experimental data (coloured crosses, left), in connection with the corresponding, duty-cycle-dependent temperature gradients as computed along the active fibre (right)

## 7 Conclusions

The results provided by our self-consistent model, proposed in view of a deeper understanding of the physics of ageing in high-power YDFAs and for explaining the related basis, have evidenced a good agreement with the experimental data of reference. This involves fairly generic trends from the state of the art, as well as our measurements dedicated to the benchmark of seed-dependent phenomena. The need for coupling pump and signal contributions, as parts of the global ageing rate, has been clearly demonstrated. Appropriate fits between our computational results and the seed-dependent variations experimented actually help to validate the principle of a natural competition between photo-darkening and photo-bleaching effects, all along the fibre. The physics of concern makes use of the actual interplay between the excited states of aggregated ions, in the form of pairs, and of the co-existing colour centres. This ensures a strong thermal coupling between neighbouring energy levels across the bottom area of gap of the silica. Highly efficient charge-transfer phenomena then occur from the trivalent ions, comprised in the pairs of interest in our simplified scheme. This leads to reduction-like phenomena associated with the basically trivalent Yb ions, thus producing divalent ions in excess. This kind of behaviour is quite consistent with already published results. It also helps to explain the dependency of the ageing rate with seeding conditions, on the point of view of the transients and subsequent duty-cycle effects. Comprehensive, space-time computational results then permit to put numbers on the seed-dependent variations which have been evidenced during the ageing process of the YDFA under test.

Representative modelling conditions essentially imply the definition of a set of four parameters. They consist of the rates of energy transfer for ETU and CT, and of the cross sections for MPA- and IR-based optical absorption by colour centres. Relevant rate values are stated for ETU and CT thanks to fitting the experiments. Referring to our notations, and to keep the numbers in mind, this applies to the set of numerical data  $\{W, W_p, \sigma_{ad}, \sigma_{aCC}\} = \{10^{-19} \text{ m}^3/\text{s}, 5 \cdot 10^{-19} \text{ m}^3/\text{s}, 10^{-27} \text{ m}^2, 10^{-23} \text{ m}^2\}$ . These data might be confirmed thanks to complementary experiments, for possible refinements or updates. This will be the topic of further work, by adding processes based on the implementation of time-resolved spectroscopy. In this respect, for evidencing complementary seed-dependent gradients and the transients of interest, space-time monitoring should apply to absorption and emission in the visible band. On the other step, aiming to more rigorous theory in terms of the physics, a variety of higher-energy levels associated with higher-order Yb clusters might be added in our very basic energy diagram. Additional energy transfers can be combined with those of current concern in the region of 2.54 eV. They should involve, more especially, the resonant line located at 3.1 eV which takes place in the absorption spectrum of Yb<sup>2+</sup>-related colour centres. More comprehensive technological data regarding the fibre-processing conditions, about the co-doping and impurity content, might bring additional answers to technology-dependent open questions. They will enable, more especially, appropriate upgrades for a finer description of the process of MPA and the determination of the exact nature of intrinsic defect centres. This implies a fractional content of co-existing divalent species

prior ageing, to be possibly specified given the availability of technological data about the fabrication of the preform of the fibre.

Our simplified approach already gives, nevertheless, an efficient basis to go on with a deeper understanding of the ageing kinetics in YDFAs. The basic principles which have been suggested will take place in further discussions of the process-dependent criteria with people involved in the fabrication of doped fibres.

**Acknowledgements** The *Conseil-Régional-d'Aquitaine* is greatly acknowledged. This work was made possible within the framework of the *S.E.M.L. Route-des-Lasers*, for supporting programmes dedicated to emerging applications in the laser industry. Many thanks also to Dr S. Vidal from *ALPhANOV*, for useful advice and comments.

## References

- C. Jauregui, T. Eidam, J. Limpert, A. Tünnermann, Impact of modal interference on the beam quality of high-power fiber amplifiers. *Opt. Express* **19**(4), 3258–3271 (2011)
- H.-J. Otto, N. Modsching, C. Jauregui, J. Limpert, A. Tünnermann, Impact of photo-darkening on the mode instability threshold. *Opt. Express* **23**(12), 15265–15277 (2015)
- M. Leich, U. Ropke, S. Jetschke, S. Unger, V. Reichel, J. Kirchhof, Non isothermal bleaching of photo-darkened Yb-doped fibers. *Opt. Express* **17**(15), 12588–12593 (2009)
- R. Piccoli, T. Robin, T. Brand, U. Klotzbach, S. Taccheo, Effective photo-darkening suppression in Yb-doped fibre lasers by visible light injection. *Opt. Express* **22**(7), 7638–7643 (2014)
- J. Kirchhof, S. Unger, A. Schwuchow, S. Jetschke, V. Reichel, M. Leich, A. Scheffel, The influence of Yb<sup>2+</sup> ions on optical properties and power stability of ytterbium doped laser fibers. *Proc. SPIE* **7598B1**, 7598B1 (2010)
- M. Engholm, S. Rydberg, K. Hammarling, Strong excited state absorption (ESA) in Yb-doped fiber lasers. *Proc. SPIE* **8601**, 86010 P-1 (2013)
- W.P. Qin, Z.Y. Liu, C.F. Wu, G.S. Qin, Z. Chen, K.Z. Zheng, Multi-ion cooperative processes in Yb<sup>3+</sup> clusters. *Light Sci. Appl.* **3**, e193 (2014). <http://www.nature.com-Open>
- S. Jetschke, A. Schwuchow, S. Unger, “Transient absorption in pumped Yb-fibers opens a path to photo-darkening. *Laser Phys. Lett.* **11**, 085101 (2014)
- J. Bouillet, C. Vinçont, C. Aguergaray, and A. Jolly, ‘Regime-dependence of photo-darkening-induced modal degradation threshold in high power photonic crystal fiber amplifier,’ *proc. ASSP– Boston-USA* (2016)
- S. Jetschke, S. Unger, U. Röpke, J. Kirchhof, Photo-darkening in Yb doped fibers: experimental evidence of equilibrium states depending on the pump power. *Opt. Express* **15**(22), 14838–14843 (2007)
- F. Mady, J.-B. Duchez, Y. Mebrouk, M. Benabdesselam, A physical model of the photo- and radiation-induced degradation of ytterbium-doped silica optical fibre. *Fundam. Appl. Silica Adv. Dielect. AIP Conf. Proc.* **1624**, 87–94 (2014)
- K.E. Mattson, The three-electron bond SiO<sub>2</sub>: Yb absorption center of pre-darkened ytterbium-doped silica. *Opt. Express* **21**(10), 12849–12864 (2013)
- A.A. Rybaltovsky, A.A. Umnikov, K.K. Bobkov, D.S. Lipatov, A.N. Romanov, M.E. Likhachev, V.B. Sulimov, A.N. Guryanov, M.M. Bubnov, E.M. Dianov, Role of oxygen hole centres in the photo-darkening of ytterbium-doped phosphor-silicate fibre. *Quantum Electr.* **43**(11), 1037–1042 (2013)
- A. Jolly, C. Vinçont, J. Bouillet, Photo-darkening kinetics in a high-power YDFA versus CW or short-pulse seed-conditions 10083-64. *Proc. SPIE* **10083**, 100831T (2017)
- H. Gebavi, S. Taccheo, D. Milanese, A. Monteville, O. Le Goffic, D. Landais, D. Mechin, D. Tregoaat, B. Cadier, T. Robin, Temporal evolution and correlation between cooperative luminescence and photo-darkening in ytterbium doped silica fibers. *Opt. Express* **19**(25), 25077–25083 (2011)
- M. Engholm, L. Norin, Preventing photo-darkening in ytterbium-doped high power lasers; correlation to the UV-transparency of the core glass. *Opt. Express* **16**(2), 1260–1268 (2008)
- L. Skuja, H. Hosono, M. Hirano, Laser-induced color centers in silica, in *Laser-Induced Damage in Optical Materials*, vol. 4347, ed. by G.J. Exarhos, A.H. Guenther, M.R. Kozlowski, K.L. Lewis, M.J. Soileau (SPIE, 2001)
- A.A. Rybaltovsky, K.K. Bobkov, V.V. Velmiskin, A.A. Umnikov, I.A. Shestakova, A.N. Guryanov, M.E. Likhachev, M.M. Bubnov, E.M. Dianov, The Yb-doped alumino-silicate fibers photo-darkening mechanism based on the charge-transfer state excitation. *Proc. SPIE* **8961**, 896116-1 (2014)
- K.K. Bobkov, A.A. Rybaltovsky, V.V. Velmiskin, M.E. Likhachev, M.M. Bubnov, E.M. Dianov, A.A. Umnikov, A.N. Guryanov, N.N. Vechkanov, I.A. Shestakova, Charge-transfer state excitation as the main mechanism of the photo-darkening process in ytterbium-doped alumino-silicate fibres. *Quantum Electr.* **44**, 1129–1135 (2014)
- R. Peretti, A.-M. Jurdyc, C. Gonnet, A new vision of photo-darkening in Yb-doped fibers. *Proc. SPIE* **8257**, 825705-1 (2012)
- S. Rydberg, M. Engholm, Experimental evidence for the formation of divalent ytterbium in the photo-darkening process of Yb-doped fiber lasers. *Opt. Express* **21**(6), 6681–6688 (2013)
- S. Liu, S. Zheng, C. Tang, X. Li, W. Xu, Q. Sheng, D. Chen, Photoluminescence and radio-luminescence properties of Yb<sup>2+</sup>-doped silica glass. *Mat. Lett.* **144**, 43–45 (2015)
- T. Kitabayashi, M. Ikeda, M. Nakai, K. Himeno, K. Obashi, Population inversion factor dependence of photo-darkening of Yb-doped fibers and its suppression by high aluminium-doping. *OFC/NFOE Conf. CD ROM (OSA, Washington-DC)* **OThC5B** (2006)
- N. Gayathri, B. Bagchi, Non-Marcus energy gap dependence of electron transfer rate in contact ion pairs. Novel interplay between relaxation and reaction in solution. *J. Mol. Struct. (Theochem)* **361**, 117–122 (1996)
- J.M. Collins, B. Di Bartolo, Temperature and energy gap dependence of energy transfer between rare-earth ions in solids. *J. Luminesc.* **69**, 335–341 (1996)